*Supplementary Materials*

Chiral or Luminescent Lanthanide Single-Molecule Magnets Involving Bridging Redox Active Triad Ligand

Bertrand Lefeuvre, Jessica Flores Gonzalez, Carlo Andrea Mattei, Vincent Dorcet, Olivier Cador and Fabrice Pointillart *

ISCR (Institut des Sciences Chimiques de Rennes)—UMR-CNRS 6226, Univ Rennes, 35000 Rennes, France; bertrand.lefeuvre@univ-rennes1.fr (B.L.); jessica.flores-gonzales@univ-rennes1.fr (J.F.G.); carlo-andrea.mattei@univ-rennes1.fr (C.A.M.); vincent.dorcet@univ-rennes1.fr (V.D.); olivier.cador@univ-rennes1.fr (O.C.)

*   Correspondence: fabrice.pointillart@univ-rennes1.fr; Tel.: +33-(0)2-23-23-57-62; Fax: +33-(0)2-23-23-68-40
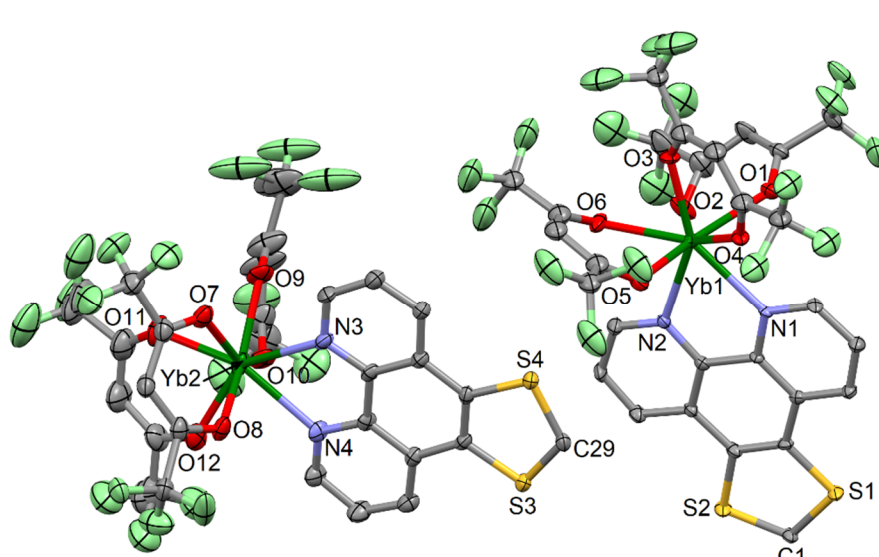
Figure S1. ORTEP view of the asymmetric unit for (**1**)·2(C_7H_{16}). Thermal ellipsoids are drawn at 30% probability. Hydrogen atoms and solvent molecules of crystallization are omitted for clarity.
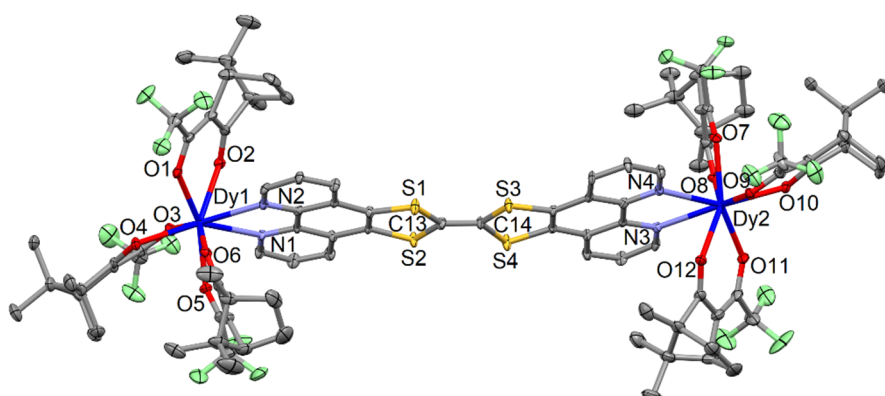
Figure S2. ORTEP view of the asymmetric unit for (**2**)·2(C_6H_{14}). Thermal ellipsoids are drawn at 30% probability. Hydrogen atoms and solvent molecules of crystallization are omitted for clarity.
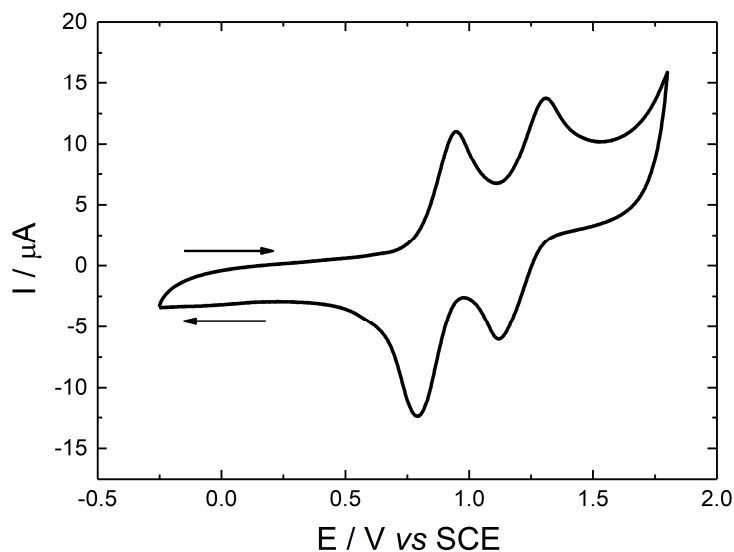
Figure S3. Cyclic voltammograms of **1** in CH_2Cl_2 at a scan rate of 100 mV·s^{-1}. The potentials were measured *vs.* a saturated calomel electrode (SCE) with Pt wires as working and counter electrodes.
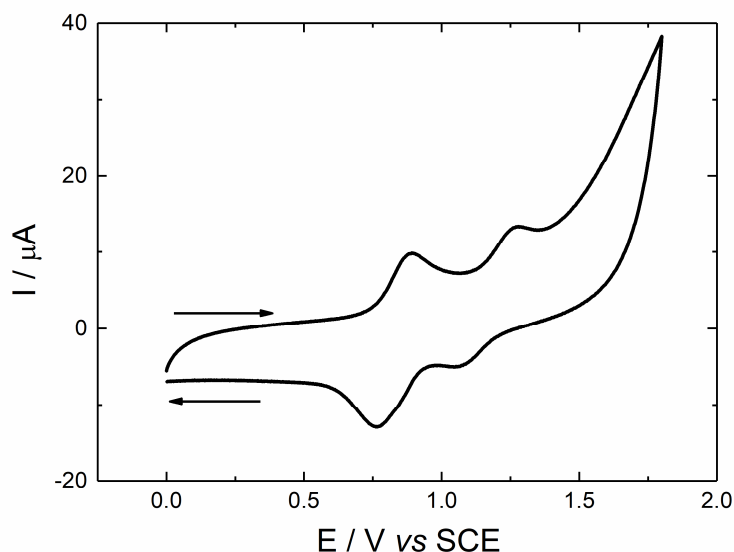
Figure S4. Cyclic voltammetry of **2** in CH_2Cl_2 at a scan rate of 100 mV·s^{-1}. The potentials were measured *versus* a saturated calomel electrode (SCE) with Pt wire as the counter electrodes.
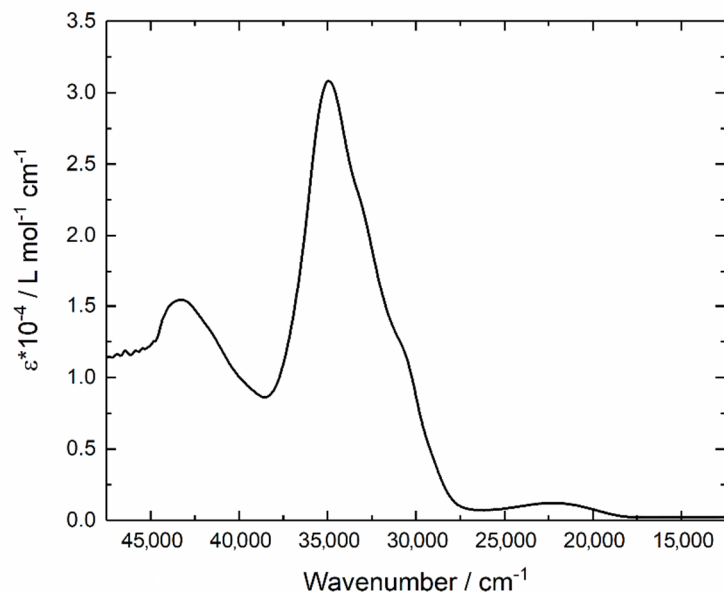
Figure S5. Experimental UV-visible absorption spectrum at room temperature of **1** in CH$_2$Cl$_2$ solution (C = 4 × 10^{-5} mol L^{-1}).
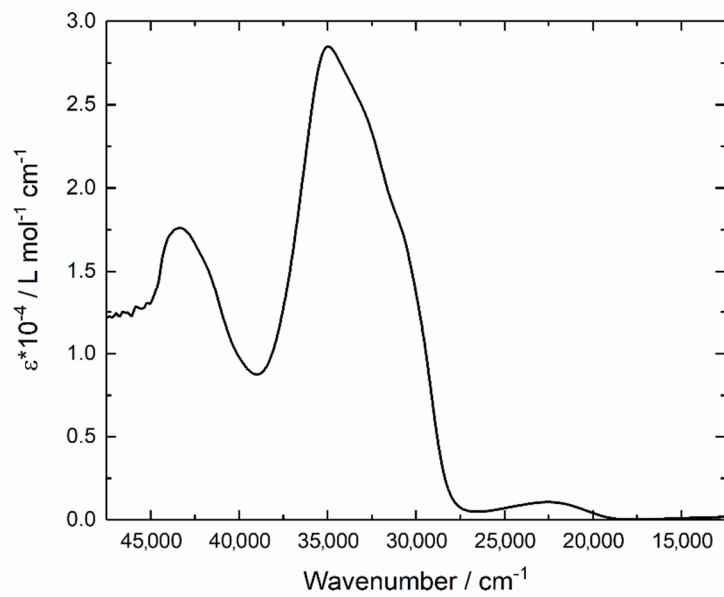
Figure S6. Experimental UV-visible absorption spectrum at room temperature of **2** in CH$_2$Cl$_2$ solution (C = 4 × 10^{-5} mol L^{-1}).
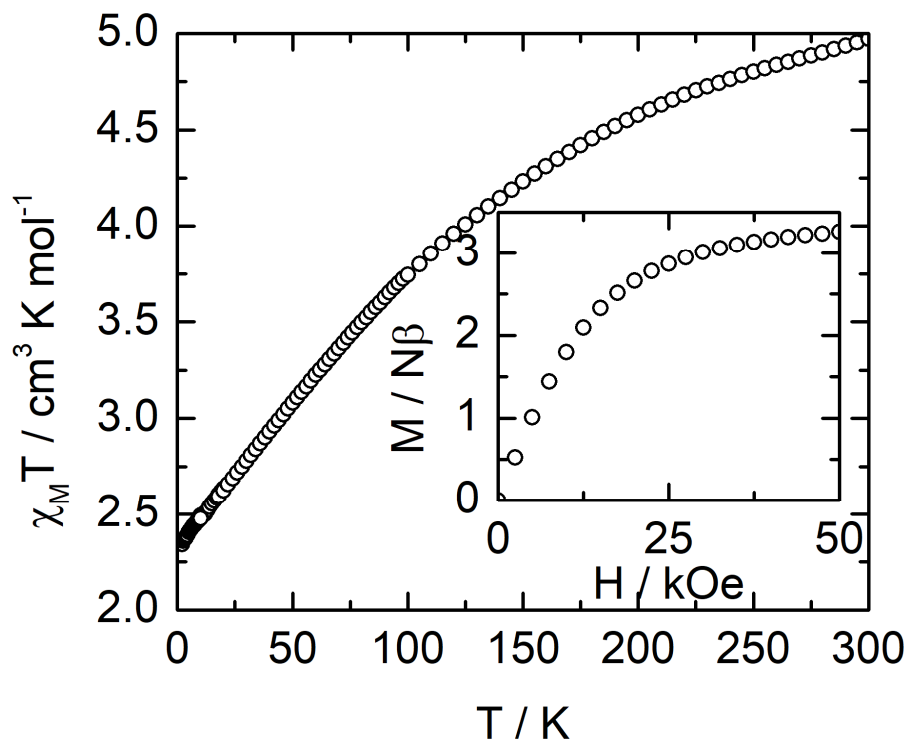
Figure S7. Thermal dependence of the $\chi_M T$ product between 2 and 300 K for **1**. In inset, field dependence of the magnetization at 2 K for **1**.
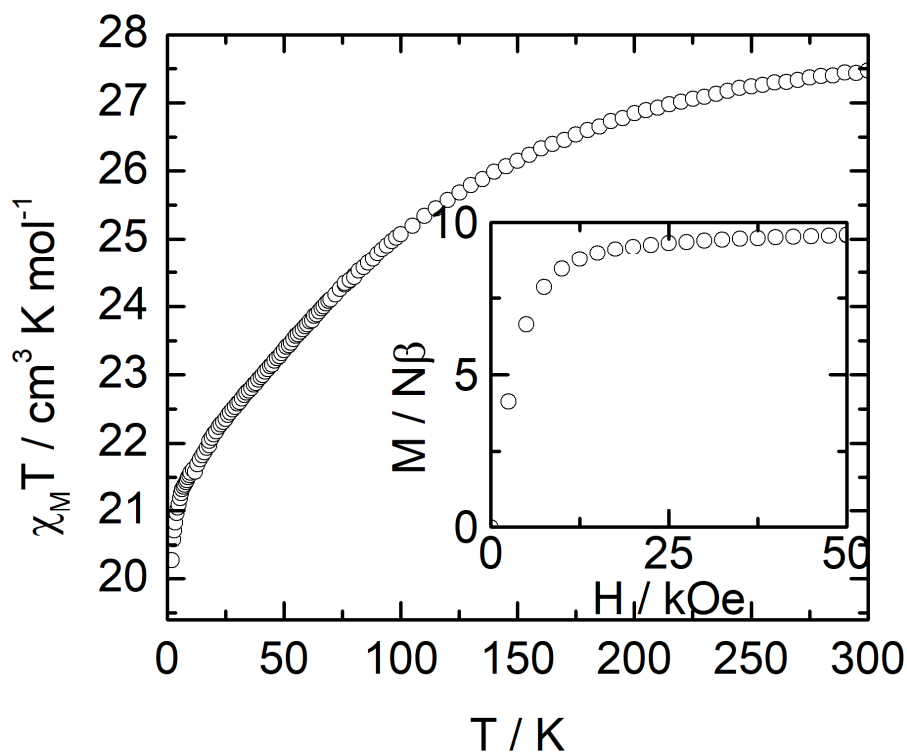
Figure S8. Thermal dependence of the $\chi_M T$ product between 2 and 300 K for **2**. In inset, field dependence of the magnetization at 2 K for **2**.
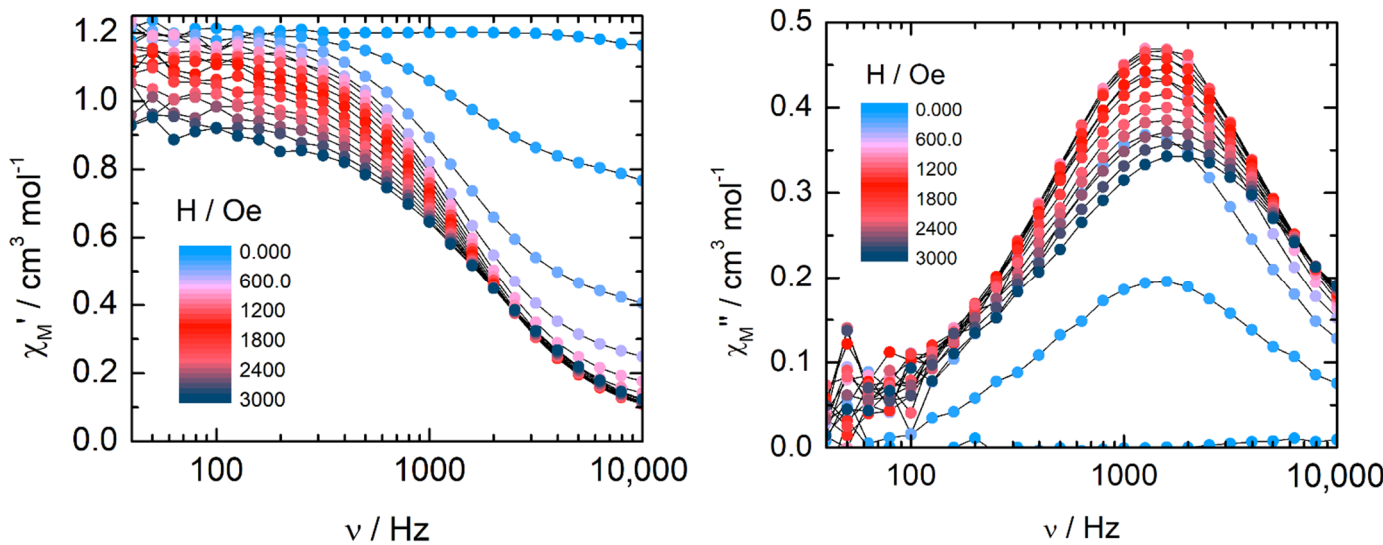
Figure S9. In-phase (left) and out-of-phase (right) components of the ac magnetic susceptibility for **1** at 2 K under a DC magnetic field from 0 to 3000 Oe.
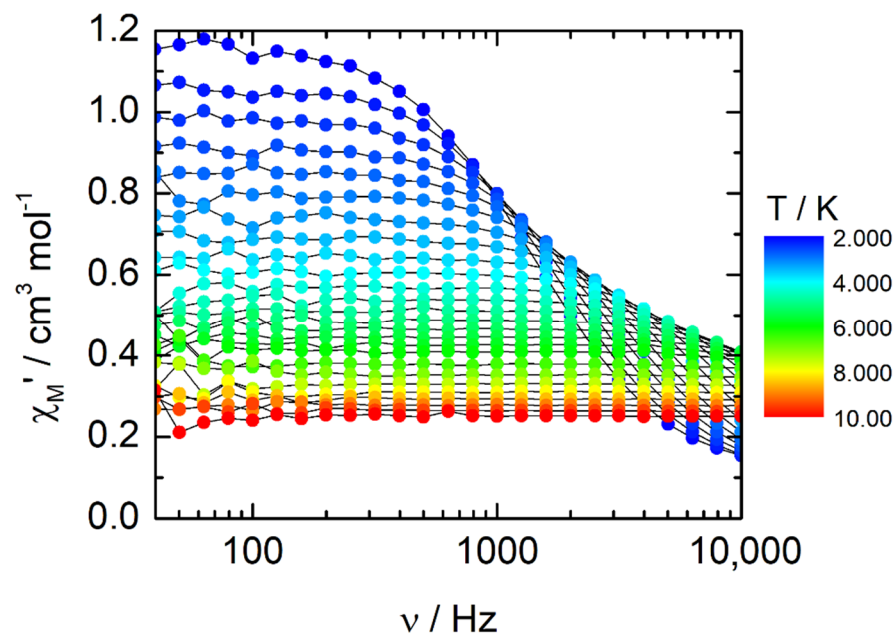
Figure S10. Frequency dependence of the in-phase component of the magnetic susceptibility under an applied magnetic field of 1000 Oe between 2 and 10 K for **1**.

Extended Debye model.

$$\chi_M' = \chi_S + \left(\chi_T - \chi_S\right) \frac{1 + \left(\omega\tau\right)^{1-\alpha} \sin\left(\alpha\frac{\pi}{2}\right)}{1 + 2\left(\omega\tau\right)^{1-\alpha} \sin\left(\alpha\frac{\pi}{2}\right) + \left(\omega\tau\right)^{2-2\alpha}}$$

$$\chi_M'' = \left(\chi_T - \chi_S\right) \frac{\left(\omega\tau\right)^{1-\alpha} \cos\left(\alpha\frac{\pi}{2}\right)}{1 + 2\left(\omega\tau\right)^{1-\alpha} \sin\left(\alpha\frac{\pi}{2}\right) + \left(\omega\tau\right)^{2-2\alpha}}$$

With χ_T the isothermal susceptibility, χ_S the adiabatic susceptibility, τ the relaxation time and α an empiric parameter which describe the distribution of the relaxation time. For SMM with only one relaxing object α is close to zero. The extended Debye model was applied to fit simultaneously the experimental variations of χ_M' and χ_M'' with the frequency ν of the oscillating field ($\omega = 2\pi\nu$). Typically, only the temperatures for which a maximum on the χ_M'' vs. ν curves, have been considered. The best fitted parameters τ, α, χ_T, χ_S are listed in Tables S5–S9 with the coefficient of determination R^2.
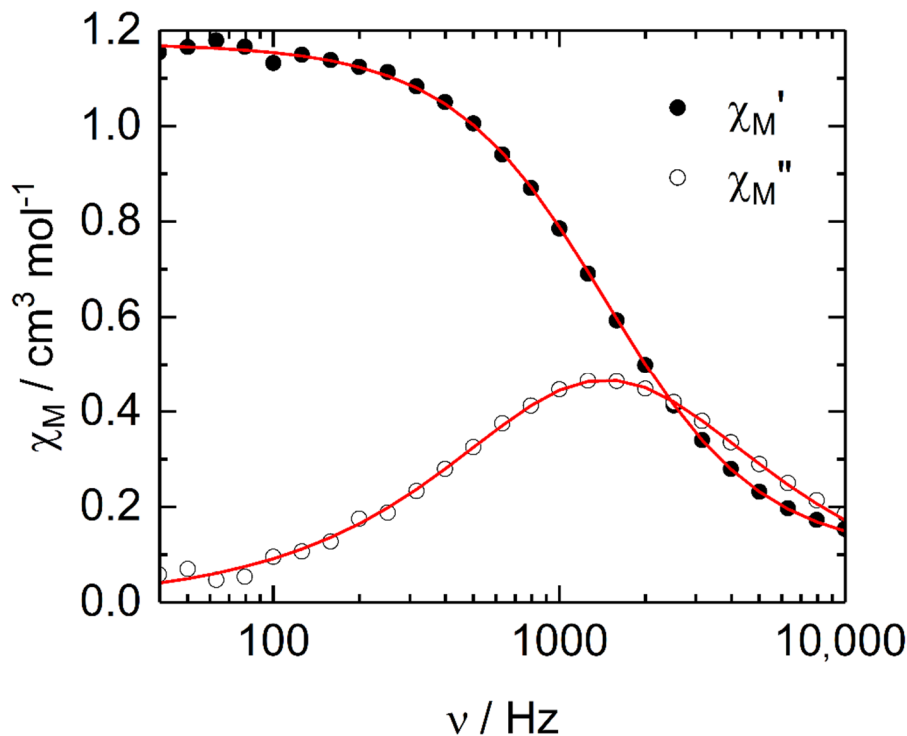
Figure S11. Frequency dependence of the in-phase (χ_M') and out-of-phase (χ_M'') components of the ac susceptibility measured on powder at 2 K and 1000 Oe with the best fitted curves (red lines) for **1**.
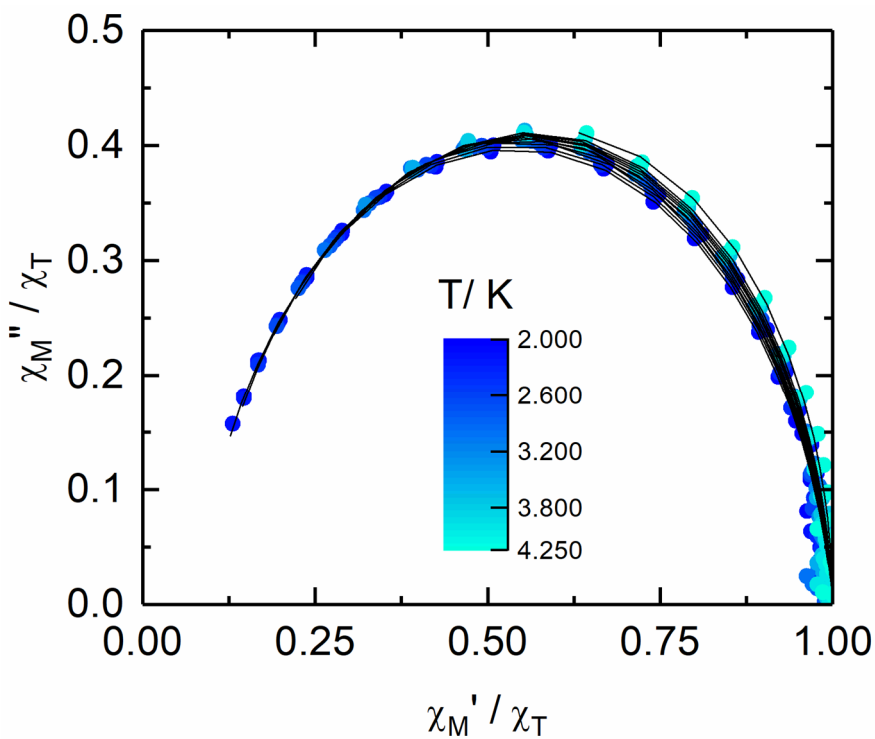
Figure S12. Normalized Cole-Cole plot for **1** at several temperatures between 2 and 4.25 K under an applied magnetic field of 1000 Oe. Black lines are the best fitted curves.
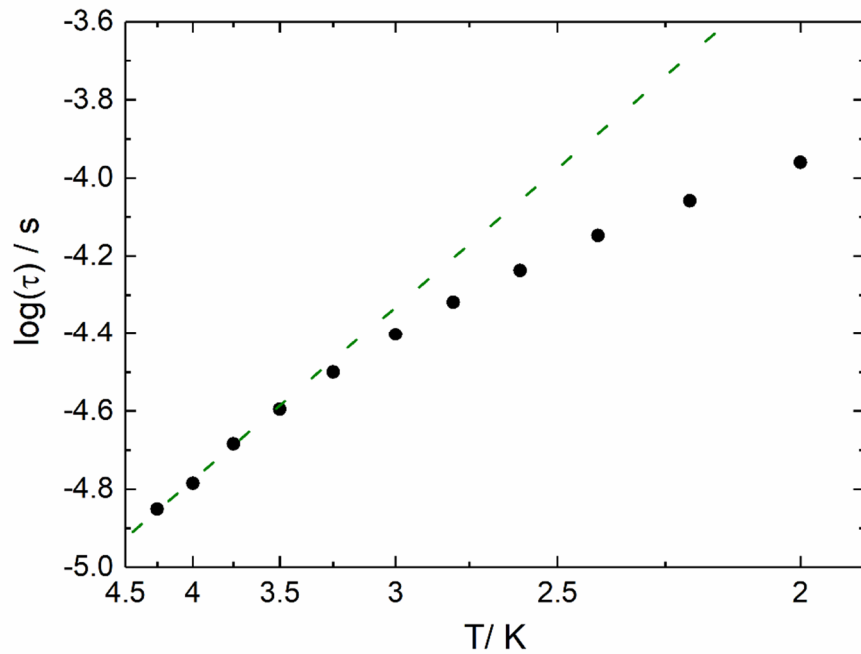
Figure S13. Temperature dependence of the relaxation time for **1** at 1000 Oe in the temperature range 2–4.25 K. Green dashed lines corresponds to the thermally activated contribution (Orbach process with the parameters given in the main text).
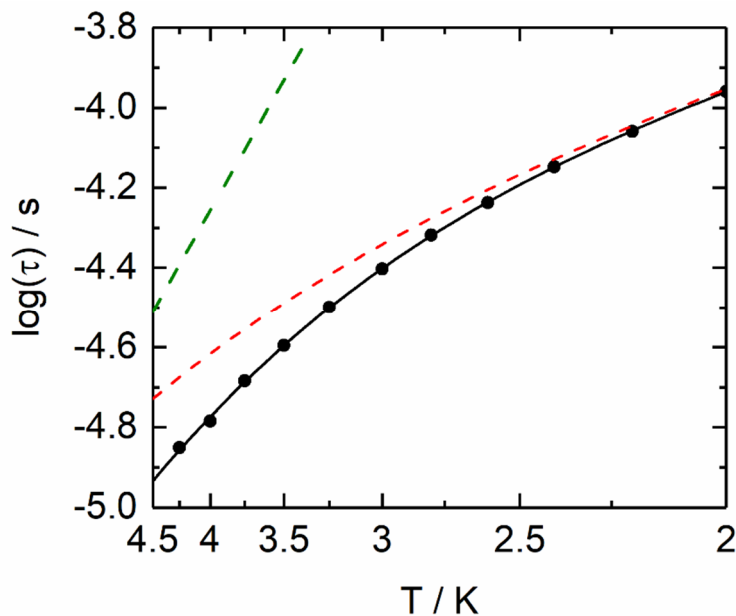
Figure S14. Temperature dependence of the relaxation time for **1** at 1000 Oe in the temperature range of 2–4.25 K with the best-fitted curve (full black line) with the combination Orbach + Raman processes. The Orbach and Raman contributions to the relaxation time are respectively represented in dashed green line and dashed red line (the parameters are given in the main text).
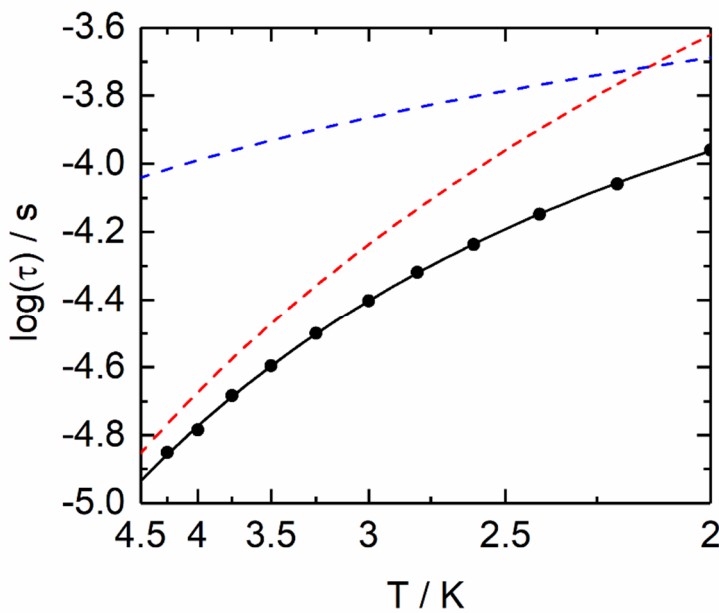
Figure S15. Temperature dependence of the relaxation time for **1** at 1000 Oe in the temperature range of 2–4.25 K with the best-fitted curve (full black line) with the combination Raman + direct processes. The Raman and direct contributions to the relaxation time are respectively represented in dashed red line and dashed blue line (the parameters are given in the main text).
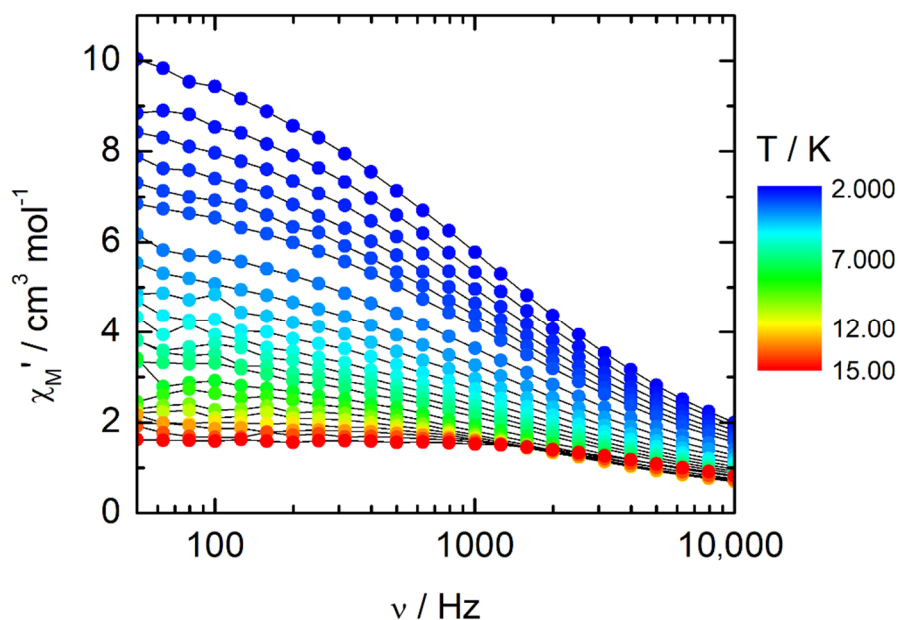
Figure S16. Frequency dependence of the in-phase component of the magnetic susceptibility under a zero applied magnetic field between 2 and 15 K for **2**.
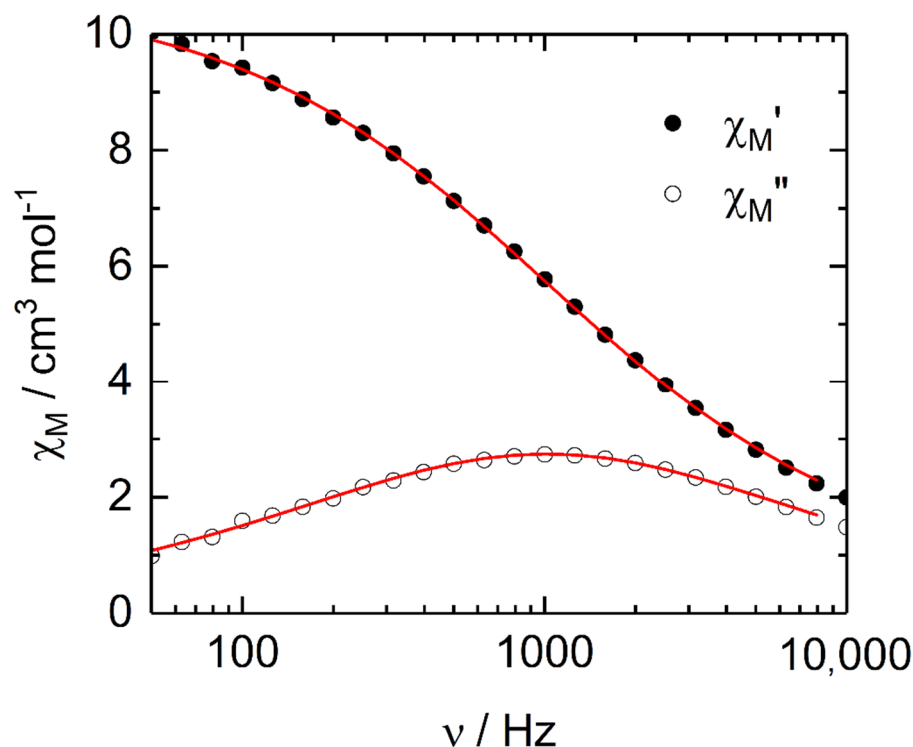

Figure S17. Frequency dependence of the in-phase (χ_M') and out-of-phase (χ_M'') components of the ac susceptibility measured on powder at 2 K in zero applied dc field with the best fitted curves (red lines) for **2**.
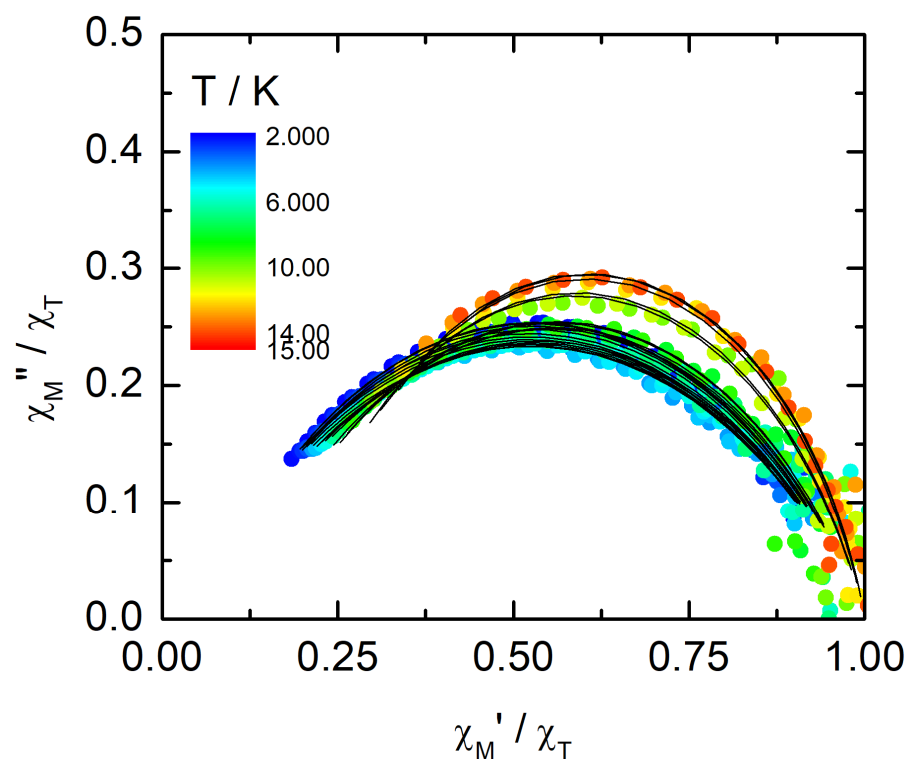
Figure S18. Normalized Cole-Cole plot for **2** at several temperatures between 2 and 15 K under a zero applied magnetic field. Black lines are the best fitted curves.
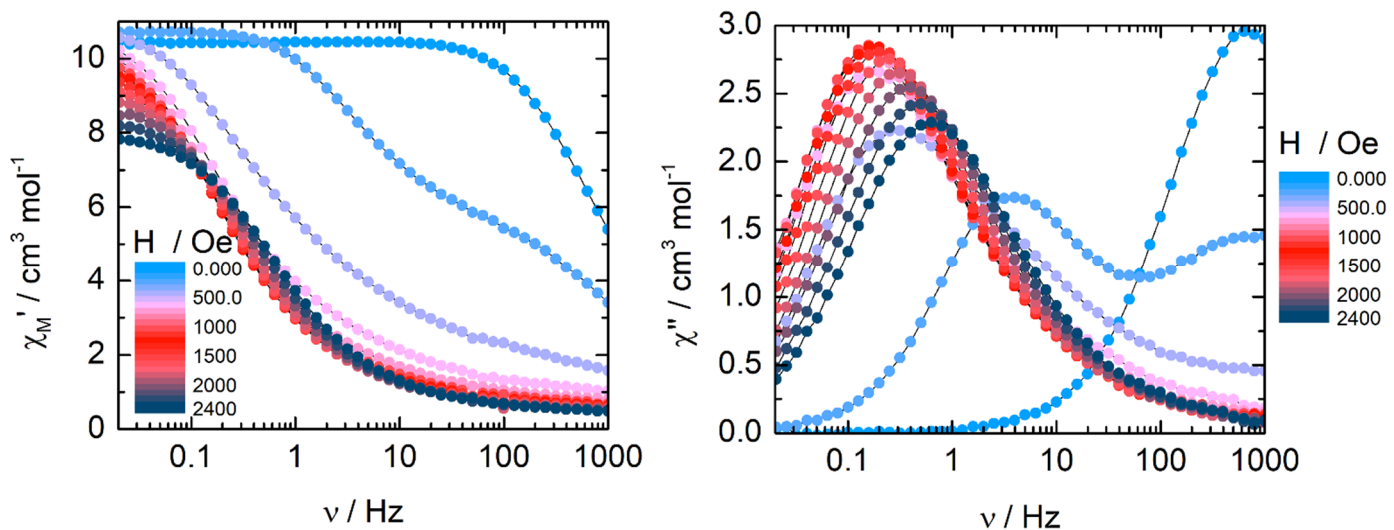
Figure S19. In-phase (**left**) and out-of-phase (**right**) components of the ac magnetic susceptibility for **2** at 2 K under a DC magnetic field from 0 to 2400 Oe.
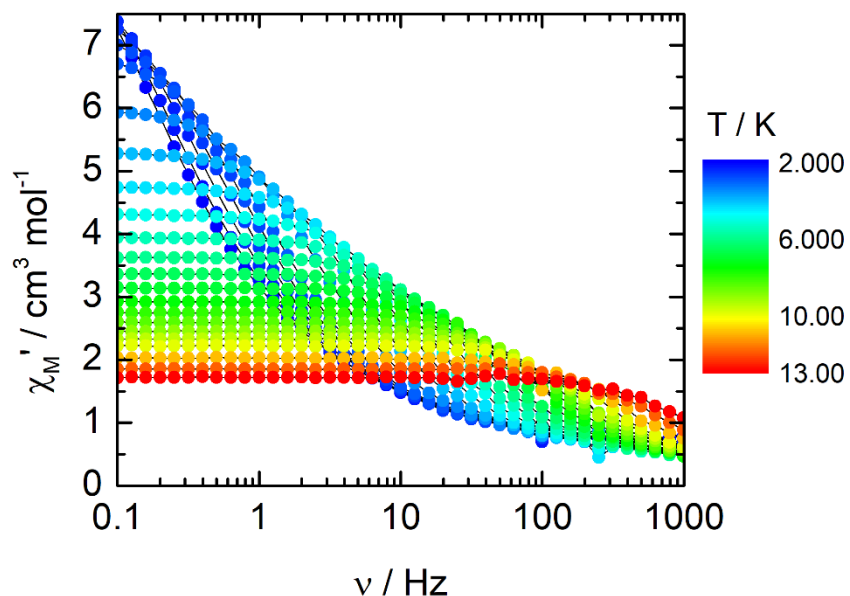
Figure S20. Frequency dependence of the in-phase component of the magnetic susceptibility under a 1200 Oe applied magnetic field between 2 and 13 K for **2**.
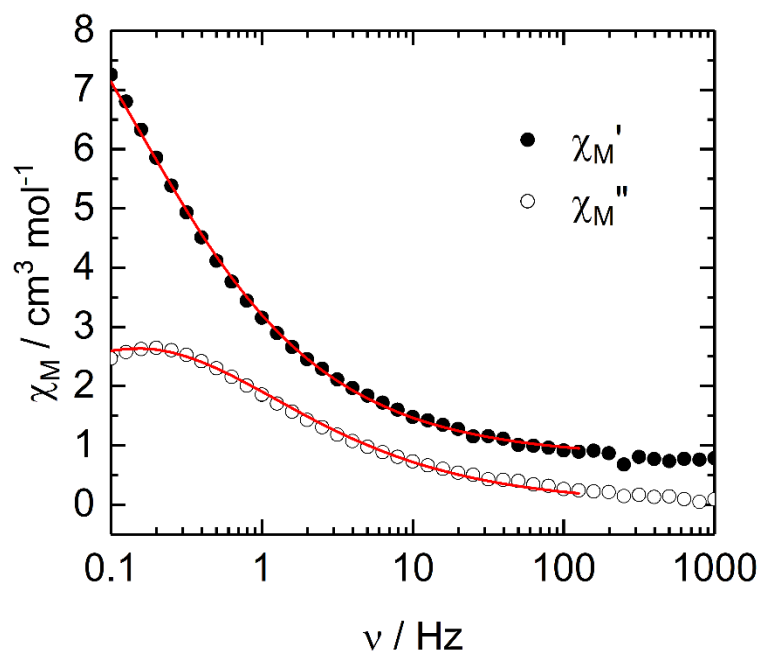
Figure S21. Frequency dependence of the in-phase (χ_M') and out-of-phase (χ_M'') components of the ac susceptibility measured on powder at 2 K and 1200 Oe with the best fitted curves (red lines) for **2**.
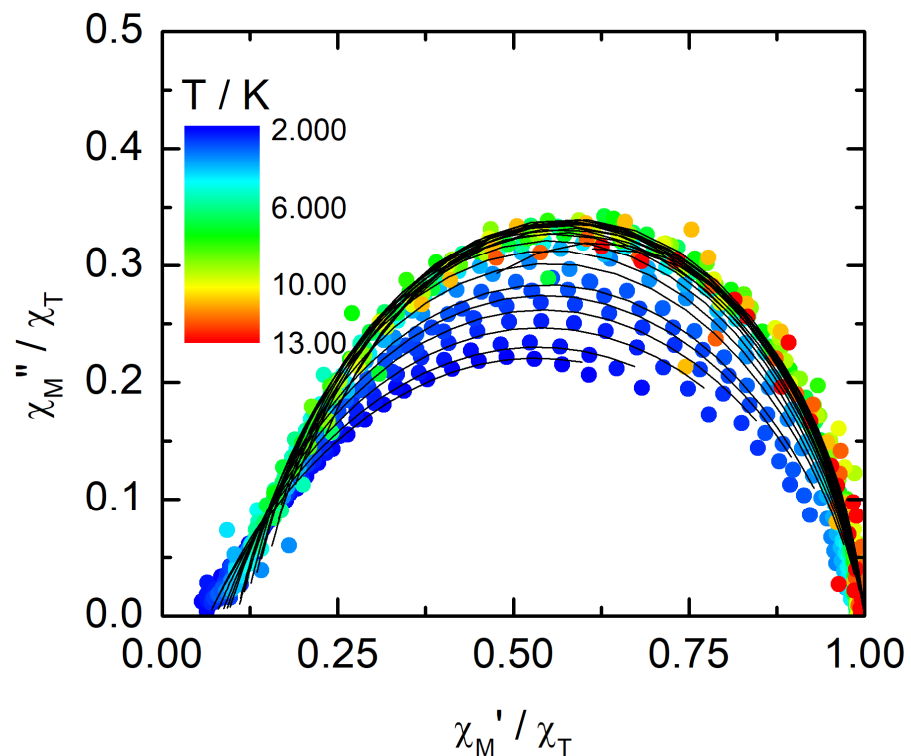
Figure S22. Normalized Cole-Cole plot for **2** at several temperatures between 2 and 13 K under a 1200 Oe applied magnetic field. Black lines are the best fitted curves.
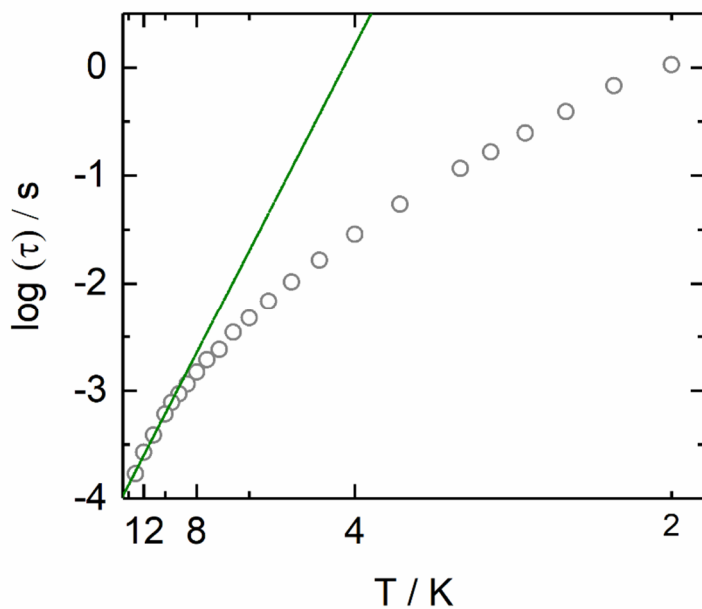
Figure S23. Temperature dependence of the relaxation time for **2** at 1200 Oe in the temperature range 2–13 K. Green line corresponds to the thermally activated contribution (Orbach process with the parameters given in the main text).
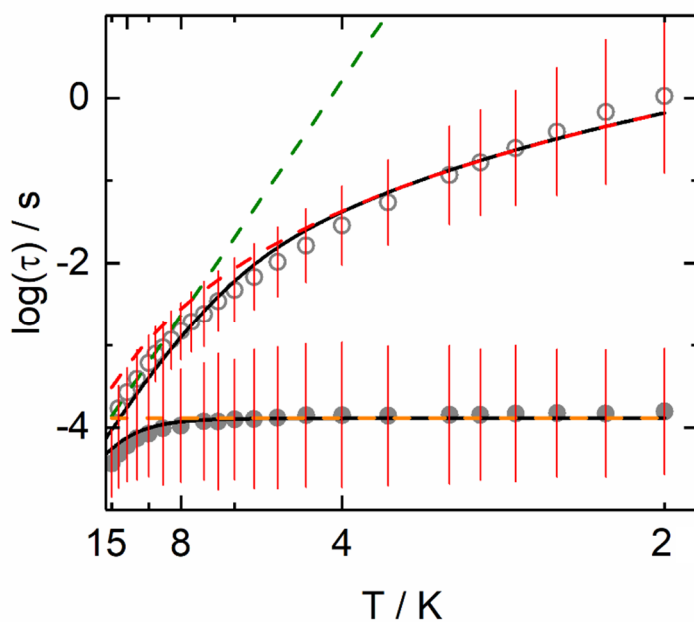
Figure S24. Temperature dependence of the relaxation time for **2** at 0 Oe (full gray cicles) and 1200 Oe (open gray circles) in the temperature range of 2–15 K with the best-fitted curve (full black line) with the combination Orbach + Raman + QTM (for H = 0 Oe) processes. The Orbach, Raman and QTM contributions to the relaxation time are respectively represented in dashed green line, dashed red line and dashed orange line (the parameters are given in the main text).

Table S1. X-ray crystallographic data for (**1**)·2(C₇H₁₆) and (**2**)·2(C₆H₁₄).

Compounds	[Yb₂(hfac)₆(L)]·2(C₇H₁₆) (**1**)·2(C₇H₁₆)	[Dy₂((+)facam)₆(L)]·2(C₆H₁₄) (**2**)·2(C₆H₁₄)
Formula	C₇₀H₅₀Yb₂F₃₆N₄O₁₆S₄	C₁₁₀H₁₂₄Dy₂F₁₈N₄O₁₂S₄
M/g.mol^{-1}	2297.26	2489.02
Crystal system	Triclinic	Monoclinic
Space group	P-1 (N°2)	C2 (N°5)
Cell parameters	a = 13.8546(16) Å b = 16.6640(20) Å c = 19.810(20) Å α = 68.703(4) ° β = 73.736(4) ° γ = 84.138 °	a = 36.4090(30) Å b = 16.7945(14) Å c = 20.6077(14) Å β = 109.051(2) °
Volume/Å³	4090.8(8)	11910.9(16)
Z	2	4
T/K	294 (2)	150(2)
2θ range /°	4.28 ≤ 2θ ≤ 55.25	5.94 ≤ 2θ ≤ 54.97
ρcalc/g.cm^{-3}	1.784	1.292
μ/mm^{-1}	2.513	1.394
Number of reflections	87776	139809
Independent reflections	18753	27186
Rint	0.0474	0.0541
Fo² > 2σ(Fo)²	14786	22607
Number of variables	1055	1226
R1, ωR2	0.0786, 0.1807	0.0384, 0.0740

Table S2. SHAPE analysis of the coordination polyhedra around the lanthanide in the polymeric compounds.

Compounds	Metal	CShM$_{SAPR-8}$ (square antiprism D$_{4d}$)	CShM$_{BTPR-8}$ (biaugmented trigonal prism C$_{2v}$)	CShM$_{TDD-8}$ (triangular dodecahedron D$_{2d}$)
(**1**)·2(C₇H₁₆)	Yb1	3.226	1.891	0.726
	Yb2	0.804	1.727	1.292
(**2**)·2(C₆H₁₄)	Dy1	0.611	1.987	2.274
	Dy2	0.582	2.298	2.012

Table S3. Selected bond lengths for (**1**)·2(C₇H₁₆) and (**2**)·2(C₆H₁₄) in Å.

(**1**)·2(C₇H₁₆)		(**2**)·2(C₆H₁₄)	
Yb1-N1	2.486(6)	Dy1-N1	2.553(5)
Yb1-N2	2.482(6)	Dy1-N2	2.561(7)
Yb1-O1	2.283(6)	Dy1-O1	2.295(5)
Yb1-O2	2.245(7)	Dy1-O2	2.418(5)
Yb1-O3	2.264(6)	Dy1-O3	2.278(6)
Yb1-O4	2.316(6)	Dy1-O4	2.347(5)
Yb1-O5	2.279(7)	Dy1-O5	2.293(4)
Yb1-O6	2.330(6)	Dy1-O6	2.371(6)
Yb2-N3	2.460(8)	Dy2-N3	2.560(6)
Yb2-N4	2.494(8)	Dy2-N4	2.560(5)
Yb2-O7	2.302(8)	Dy2-O7	2.316(4)
Yb2-O8	2.299(7)	Dy2-O8	2.363(6)

Yb2-O9	2.241(7)	Dy2-O9	2.273(6)
Yb2-O10	2.289(8)	Dy2-O10	2.352(5)
Yb2-O11	2.263(7	Dy2-O11	2.295(5)
Yb2-O12	2.303(9)	Dy2-O12	2.400(5)

Table S4. Oxidation potentials of the complexes **1** and **2** (V *vs* SCE, nBu$_4$NPF$_6$, 0.1 M in CH$_2$Cl$_2$ at 100 mV·s^{-1}).

	$E^1_{1/2}$/V		$E^2_{1/2}$/V	
	$^{ox}E^1_{1/2}$	$^{red}E^1_{1/2}$	$^{ox}E^2_{1/2}$	$^{red}E^2_{1/2}$
1	0.79	0.94	1.12	1.31
2	0.77	0.89	1.06	1.28

Table S5. Best fitted parameters (χ_T, χ_S, τ and α) with the extended Debye model for compound **1** at 2 K in the magnetic field range 200–3000 Oe.

H/Oe	χ_S/cm^3 mol^{-1}	χ_T/cm^3 mol^{-1}	τ/s	α	R^2
200	0.7638	1.20519	1.05006×10^{-4}	0.06511	0.99953
400	0.38111	1.19576	1.16489×10^{-4}	0.06099	0.99894
600	0.20769	1.19323	1.17414×10^{-4}	0.07567	0.99904
800	0.12184	1.1966	1.15902×10^{-4}	0.09469	0.99916
1000	0.09218	1.16291	1.11643×10^{-4}	0.07705	0.99933
1200	0.06389	1.15369	1.10151×10^{-4}	0.09315	0.99938
1400	0.05907	1.12899	1.08828×10^{-4}	0.09026	0.99929
1600	0.03066	1.13146	1.08811×10^{-4}	0.13502	0.99869
1800	0.03416	1.10227	1.07326×10^{-4}	0.13122	0.99885
2000	0.0257	1.08217	1.05455×10^{-4}	0.14908	0.9995
2200	0.02116	1.04837	1.01673×10^{-4}	0.15667	0.99889
2400	0.01541	1.02694	9.89154×10^{-5}	0.17065	0.99731
2600	0.01915	0.99514	9.55637×10^{-5}	0.17017	0.99926
2800	0.00754	0.96996	9.08483×10^{-5}	0.19122	0.99769
3000	0.01328	0.93759	8.6781×10^{-5}	0.18679	0.99904

Table S6. Best fitted parameters (χ_T, χ_S, τ and α) with the extended Debye model for compound **1** at 1000 Oe in the temperature range 2–4.25 K.

T / K	χ_S / cm^3 mol^{-1}	χ_T / cm^3 mol^{-1}	τ / s	α	R^2
2	0.09347	1.17539	1.09694×10^{-4}	0.09371	0.99956
2.2	0.09322	1.06932	8.73066×10^{-5}	0.07876	0.99942
2.4	0.08396	0.99504	7.11925×10^{-5}	0.08516	0.99939
2.6	0.08315	0.91848	5.79604×10^{-5}	0.0744	0.99936
2.8	0.08369	0.85759	4.80018×10^{-5}	0.06663	0.99953
3	0.07812	0.80396	3.95946×10^{-5}	0.06645	0.9987
3.25	0.07894	0.74438	3.16372×10^{-5}	0.05767	0.99925
3.5	0.07718	0.69348	2.53793×10^{-5}	0.05243	0.99927
3.75	0.08336	0.64617	2.07009×10^{-5}	0.03661	0.99846
4	0.0717	0.60939	1.64068×10^{-5}	0.04608	0.99951
4.25	0.09275	0.56677	1.40916×10^{-5}	0.00638	0.99704

Table S7. Best fitted parameters (χ_T, χ_S, τ and α) with the extended Debye model for compound **2** at 0 Oe in the temperature range 2–14 K.

T / K	χ_S / cm^3 mol^{-1}	χ_T / cm^3 mol^{-1}	τ / s	α	R^2
2	0.62144	10.81489	1.56848×10^{-4}	0.37103	0.99981
2.2	0.55615	9.83332	1.48231×10^{-4}	0.37351	0.99956
2.4	0.54267	9.15966	1.49025×10^{-4}	0.37654	0.99995
2.6	0.40669	8.6343	1.47913×10^{-4}	0.39682	0.99951
2.8	0.46312	7.94761	1.42658×10^{-4}	0.38346	0.99985
3	0.35609	7.57812	1.4287×10^{-4}	0.40306	0.99975
3.5	0.32741	6.61907	1.3917×10^{-4}	0.40645	0.9995
4	0.27751	5.98642	1.41778×10^{-4}	0.4201	0.99946
4.5	0.29795	5.40421	1.40793×10^{-4}	0.41504	0.9988
5	0.27713	4.84938	1.31352×10^{-4}	0.41091	0.99963
5.5	0.28506	4.42532	1.27402×10^{-4}	0.40447	0.99981
6	0.41683	3.99764	1.24825×10^{-4}	0.35565	0.99692
6.5	0.27227	3.80159	1.17991×10^{-4}	0.39669	0.99974
7	0.39818	3.5018	1.18553×10^{-4}	0.34721	0.99592
8	0.36508	3.06919	1.04991×10^{-4}	0.33518	0.99856
9	0.33816	2.80952	9.792×10^{-5}	0.33237	0.99927
10	0.42363	2.42743	8.42934×10^{-5}	0.24849	0.99751
11	0.40547	2.24926	7.41286×10^{-5}	0.23914	0.99728
12	0.41219	2.02696	6.04731×10^{-5}	0.19686	0.9976
13	0.39028	1.87834	4.79685×10^{-5}	0.18472	0.9991
14	0.38209	1.76251	3.66555×10^{-5}	0.1781	0.99663

Table S8. Best fitted parameters (χ_T, χ_S, τ and α) with the extended Debye model for compound **2** at 2 K in the magnetic field range 200–2400 Oe.

H / Oe	χ_S / cm^3 mol^{-1}	χ_T / cm^3 mol^{-1}	τ / s	α	R^2
200	0.16073	2.57351	0.04662	0.17685	0.99991
400	0.94027	7.10845	0.32873	0.51658	0.99733
600	0.63668	7.07133	0.747	0.45335	0.99771
800	0.52229	6.87458	0.86705	0.41637	0.9981
1000	0.46183	6.64219	0.84806	0.3918	0.99825
1200	0.42581	6.38269	0.77013	0.37101	0.99845
1400	0.40214	6.13232	0.67025	0.35399	0.99858
1600	0.37745	5.86072	0.5584	0.34098	0.99879
1800	0.36148	5.59157	0.45422	0.33005	0.999
2000	0.34285	5.32637	0.36271	0.32385	0.99907
2200	0.32545	5.05932	0.28662	0.32275	0.99931
2400	0.31288	4.79722	0.22604	0.32177	0.99943

Table S9. Best fitted parameters (χ_T, χ_S, τ and α) with the extended Debye model for compound **2** at 1200 Oe in the temperature range 2-13 K.

T / K	χ_S / cm^3 mol^{-1}	χ_T / cm^3 mol^{-1}	τ / s	α	R^2
2	0.78645	11.94186	1.06114	0.43791	0.99901
2.2	0.71857	10.80345	0.67974	0.41669	0.99845
2.4	0.72283	9.48483	0.39238	0.37555	0.99842
2.6	0.71911	8.54961	0.24829	0.33835	0.99844
2.8	0.69809	7.82941	0.16603	0.30986	0.99866
3	0.67757	7.26918	0.11663	0.28883	0.9987
3.5	0.65754	6.18766	0.05454	0.24385	0.9986
4	0.57378	5.42461	0.02864	0.22246	0.99913
4.5	0.53116	4.83302	0.01644	0.20343	0.9992
5	0.51172	4.36524	0.01038	0.18724	0.99944
5.5	0.48801	3.98392	0.00685	0.17595	0.99941
6	0.45921	3.6628	0.00475	0.16845	0.99955
6.5	0.46422	3.39303	0.00348	0.15642	0.99963
7	0.42255	3.16799	0.00241	0.17403	0.9985
7.5	0.39414	2.94466	0.00193	0.15628	0.99932
8	0.40508	2.76526	0.00149	0.14379	0.9995
8.5	0.38548	2.60878	0.00116	0.14791	0.99971
9	0.41106	2.46697	9.34269×10^{-4}	0.1288	0.99981
9.5	0.38667	2.34654	7.80051×10^{-4}	0.13423	0.99929
10	0.36785	2.23315	6.07002×10^{-4}	0.13638	0.99961
11	0.32197	2.03157	3.86521×10^{-4}	0.14918	0.99812
12	0.44022	1.85987	2.67843×10^{-4}	0.11167	0.99944
13	0.45154	1.72191	1.70286×10^{-4}	0.10081	0.99954